International Journal of Thermal Sciences 64 (2013) 137–144

Contents lists available at SciVerse ScienceDirect

International Journal of Thermal Sciences

journal homepage: www.elsevier.com/locate/ijts

Influence of non-conducting pore inclusions on phase change behavior of porous media with constant heat flux boundary

X.H. Yang [a], T.J. Lu [b,*], T. Kim [c,*]

[a] School of Energy and Power Engineering, Xi'an Jiaotong University, Xi'an 710049, PR China
[b] State Key Laboratory for Mechanical Structure Strength and Vibration, School of Aerospace, Xi'an Jiaotong University, Xi'an 710049, PR China
[c] School of Mechanical Engineering, University of the Witwatersrand, Private Bag 3, Wits 2050, Johannesburg, South Africa

ARTICLE INFO

Article history:
Received 14 March 2012
Received in revised form
4 September 2012
Accepted 5 September 2012
Available online 11 October 2012

Keywords:
Solidification
Heterogeneous material
Thermal boundary condition
Numerical simulation

ABSTRACT

A one-dimensional analytical solution was presented for the temporal variation of phase interface in two-phase materials having randomly distributed stagnant low conducting pores with constant heat flux boundary. For validation, numerical simulations based on the finite difference method were conducted. It was demonstrated that the phase interface propagates faster with pore inclusion than that associated with constant wall temperature boundary. Such faster movement of the phase interface is attributed to the decreased effective density of the medium as a result of the included low conducting pores. The decreased effective density reduces the amount of latent heat of the medium whilst the amount of heat removed at the boundary remains constant. Therefore, at a given period of time, more latent heat is liberated. In addition, for a given porosity, the influence of pore shape upon phase change interface location is negligible since the effective conductivity, although varying considerably with pore shape, has a marginal effect on the behavior of phase change interface.

1. Introduction

Phase change problems associated with solidification or melting, collectively known as "Stefan (or Stefan-type) problems", are involved in a wide variety of practical applications such as thermal storage systems of solar energy [1], cooling/heating of buildings [2], shell-and-tube type heat exchanger systems [3], welding, heat treatment, and casting [4]. Actual thermal systems involving phase change are subject to diverse thermal conditions including constant heat flux and constant temperature at the system boundary. As the temporal behavior of phase interface that separates two distinct phases is of great practical importance, numerous efforts have been devoted to predicting its temporal variation under different thermal boundary conditions. It appears that Neumann [5] and El-Genk and Cronenberg [6] firstly reported analytical solutions capable of predicting the phase change interface location of phase change materials (PCMs) subject to either constant temperature [5] or constant heat flux [6] boundary conditions.

Besides the above two exact solutions, a number of approximate methods have been proposed to predict the temporal variation of phase interface, including: (a) quasi-steady solution [5], (b) heat balance integral method [7], (c) perturbation method [8], (d) thermal resistance method [9], (e) Megerlin method [10], and (f) try-and-error method [11]. Amongst these approximate methods, the quasi-steady solution is the simplest, yet capable of providing a reasonable accuracy for one-dimensional (1D) phase change problems particularly when the Stefan number is small ($Ste << 1$). For larger Ste numbers, however, the solution leads to relatively large discrepancies as it neglects sensible heat. To overcome such discrepancy, Lin [12] modified the quasi-steady solution by considering the effect of sensible heat.

Goodman [7] provided an approximate solution for the melting of a semi-infinite slab with constant heat flux thermal boundary using the heat balance integral method, which was later extended to many phase change problems. Stephan and Holzknecht [8] suggested that nonlinear phase change problems can be solved by the perturbation method when the Stefan number is much less than unity. In addition, the thermal resistance method [9], Megerlin method [10] and try-and-error method [11] are widely used. However, these approximate methods are effective in solving phase change problems only when the Stefan number is small. Recently, numerical methods such as the finite difference method (FDM) and the finite element method (FEM) have become popular due to their prediction accuracy and easy convergence [13].

Strictly speaking, the exact solutions (i.e., the Neumann and El-Genk and Cronenberg solutions) dealing with 1D phase change in

* Corresponding authors. Tel.: +27 011 717 7359.
E-mail addresses: tjlu@mail.xjtu.edu.cn (T.J. Lu), tong.kim@wits.ac.za (T. Kim).

1290-0729/$ – see front matter © 2012 Elsevier Masson SAS. All rights reserved.
http://dx.doi.org/10.1016/j.ijthermalsci.2012.09.005

Nomenclature

c_p	specific heat at constant pressure (J kg^{-1} K^{-1})
f_s	solid fraction
H	total thickness (or length) of PCM parallel to heat flow (m)
$\widehat{H}$	enthalpy (J)
$\widehat{h}$	sensible enthalpy (J)
k_s	thermal conductivity of solid phase of PCM (W m^{-1} K^{-1})
k_f	thermal conductivity of liquid phase of PCM (W m^{-1} K^{-1})
k_e	effective thermal conductivity of solid–liquid phase of PCM (W m^{-1} K^{-1})
L	latent heat of PCM (J kg^{-1})
PCM	phase change material
q_w''	constant heat flux at $x = 0$ (W m^{-2})
q_ξ''	heat flux at the phase interface (W m^{-2})
$q_{\xi m}''$	heat flow per unit mass defined as Q/m at the phase interface (W kg^{-1})
q_{local}''	local heat flux at certain cross-section (W m^{-2})
$S(t)$	location of phase interface front (m)
Ste	Stefan number defined as $Ste = c_p(T_0 - T_m)/L$ with constant temperature boundary
Ste''	modified Stefan number defined as $Ste'' = (c_pHq''/k_s)/L$ with constant heat flux boundary
t	time (s)
T_m	melting temperature of PCM (K)
T_s	temperature of PCM in solidified layer (K)
T_f	temperature of PCM in liquid layer (K)
$T_{solidus}$	solidus temperature of PCM (K)
$T_{liquidus}$	liquidus temperature of PCM (K)
x	axis coinciding with solidification

Greek symbols

α	thermal diffusivity of PCM (m^2 s^{-1})
ε	void fraction (porosity) of heterogeneous material
ξ	dimensionless solid–liquid phase interface location
ρ	density of PCM (kg m^{-3})
τ	dimensionless time

a semi-infinite domain are solely applicable to homogeneous materials. To reveal the physical mechanism of phase change behavior in a heterogeneous medium having constant wall temperature boundary and low conducting circular pores, an extended analytical model has recently been proposed [14–16]. It was demonstrated that the pore inclusion decelerated the solidification of the heterogeneous medium due solely to the reduction in effective thermal conductivity.

It is yet unclear how the pore inclusion affects the phase change behavior of a heterogeneous medium subject to constant heat flux boundary conditions. This study aims to investigate the temporal variation of solid–liquid interface location of a heterogeneous medium under constant heat flux. To emphasize the distinctive features associated with the constant heat flux boundary, the temporal behavior of phase interface and temperature distribution in a solidified layer is compared with that observed under constant temperature boundary. Due to mathematical complexities associated with moving boundaries and internal heat generation due to chemical reactions occurring during phase change, the present study is restricted to 1D phase change in a semi-infinite heterogeneous medium initially at the melting temperature. An analytical model is developed by combining the phase change model of El-Genk and Cronenberg [6] for homogeneous media with the effective thermal conductivity model of Bauer [17] for porous (two-phase heterogeneous) materials. To validate the model predictions, numerical simulations based on the finite difference method are performed. The influence of pore shape and porosity upon the phase change behavior is quantified.

2. Analytical approach

2.1. Phase change in a dense (homogeneous) material with constant heat flux thermal boundary

Consider first one-dimensional phase change of a homogeneous material from liquid to solid, i.e., solidification. Initially, the liquid with length (or depth) H and infinite width (for simplicity) is at melting (fusion) temperature T_m. Solidification is initiated from $x = 0$ (see Fig. 1) where a constant heat flux ($q_w'' = $ constant) is imposed at time $t \geq 0$.

The relevant physical properties of the material in either liquid or solid state such as the latent heat (L), thermal conductivity (k_s for solid phase and k_f for liquid phase), thermal diffusivity (α_s), and specific heat at constant pressure (c_p) are assumed to be invariant in temperature, time, and space, but different phases may have different properties. In addition, $S(t)$ in Fig. 1 represents the phase interface separating the melt and the solid. Under such conditions, the temperature distribution may be expressed as $T_s = T_s(x,t)$ for the solid phase (or solidified layer) and $T_f = T_m$ for the melt. Also, it is postulated that the transfer of heat within the solidified layer is solely by conduction. Then, the 1D heat conduction along the x-direction is governed by:

$$\frac{\partial T_s}{\partial t} = \alpha_s \frac{\partial^2 T_s}{\partial x^2}, \quad 0 < x < S(t) \tag{1}$$

The initial and boundary conditions are:

$$T_s(x,0) = T_m, \quad \text{at } t = 0 \tag{2}$$

$$k_s \left.\frac{\partial T_s}{\partial x}\right|_{x=0} = q_w'', \quad \text{at } x = 0 \tag{3}$$

$$T_s(x,t) = T_m, \quad \text{at } x = S(t) \tag{4}$$

$$k_s \frac{\partial T_s}{\partial x} = \rho_s L \frac{\mathrm{d}S(t)}{\mathrm{d}t}, \quad \text{at } x = S(t) \tag{5}$$

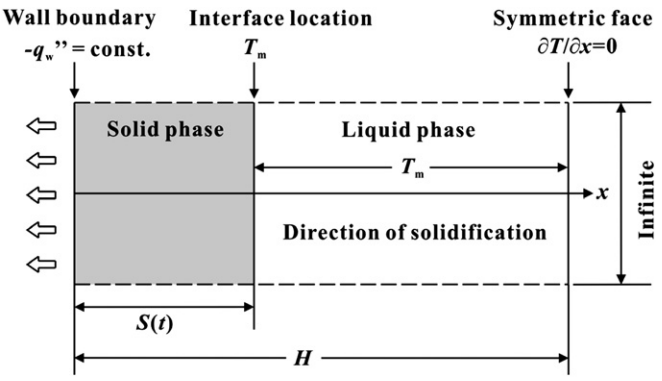

Fig. 1. Schematic of one-dimensional solidification with constant heat flux imposed at the boundary ($x = 0$).

Due to the mathematical complexities associated with nonlinear phase change problems, only a few exact analytical solutions exist for specialized cases [5]. El-Genk and Cronenberg [6] reported an exact solution for the 1D solidification (freezing) of a semi-infinite liquid initially at melting temperature. The transient temperature distribution in the solidified layer of the liquid has the form:

$$T_s(x,t) = T_m + \frac{2q''_w}{k_s}\sqrt{\alpha_s t\left[ierfc\left(\frac{S(t)}{2\sqrt{\alpha_s t}}\right) - ierfc\left(\frac{x}{2\sqrt{\alpha_s t}}\right)\right]} \quad (6)$$

Here, the phase interface location $S(t)$ must satisfy:

$$\frac{dS(t)}{dt} = \frac{q''_w}{\rho_s L}\,erfc\left(\frac{S(t)}{2\sqrt{\alpha_s t}}\right) \quad (7)$$

where $erfc(x)$ and $ierfc(x)$ are error functions defined respectively as $erfc(x) = (2/\sqrt{\pi})\int_x^\infty \exp(-\eta^2)d\eta$ and $ierfc(x) = (1/\sqrt{\pi})\exp(-x^2) - x(2/\sqrt{\pi})\int_x^\infty \exp(-\eta^2)d\eta$.

Two dimensionless parameters were introduced by El-Genk and Cronenberg [6] for the solidified layer thickness and time, respectively, as:

$$\xi(\tau) = \left(\frac{q''_w}{\alpha_s\rho_s L}\right)S(t) \quad (8)$$

$$\tau_s = \left(\frac{q''_w}{\sqrt{\alpha_s\rho_s L}}\right)^2 t \quad (9)$$

Substitution of (8) and (9) into (7) yields:

$$\frac{d\xi}{d\tau_s} = erfc\left(\frac{\xi}{2\sqrt{\tau_s}}\right) \quad (10)$$

Eq. (10) may be solved say using numerical methods for the dimensionless solid–liquid interface location. However, one of the control parameters, i.e., heat flux q_w'', is implicitly expressed in (8) and (9). Therefore, it is necessary to derive a new dimensionless form of the solid–liquid interface, which can explicitly show the heat flux term. To this end, Eqs. (8) and (9) are non-dimensionalized as:

$$\xi(\tau) = \frac{S(t)}{H} \quad (11)$$

$$\tau_s = \frac{\alpha_s t}{H^2} \quad (12)$$

A new form of the solid–liquid interface then takes the form:

$$\frac{d\xi}{d\tau_s} = Ste''erfc\left(\frac{\xi}{2\sqrt{\tau_s}}\right) \quad (13)$$

where Ste'' is the modified Stefan number defined as:

$$Ste'' = \frac{q''_w H}{\alpha_s\rho_s L} = \frac{c_p H(q''_w/k_s)}{L} = \frac{c_p H}{L}\cdot\left.\frac{dT}{dx}\right|_{x=0} \quad (14)$$

Physically, the modified Stefan number (Ste'') under constant heat flux thermal boundary is similar to the classical Stefan number ($Ste = c_p(T_0 - T_m)/L$), both denoting the ratio of sensible heat to latent heat.

2.2. Extended solutions for phase change in a heterogeneous medium

Consider next a heterogeneous medium containing randomly distributed stagnant and low conducting circular pores. To accommodate the pore inclusion analytically, several essential bulk material parameters need to be modified, including: (1) thermal conductivity k, (2) density ρ, and (3) thermal diffusivity α as a product of thermal conductivity, density and specific heat. In the following section, the modification of each parameter is discussed separately.

Bauer [17] reported a model for the effective thermal conductivity of a discrete phase medium (pore) randomly distributed in a continuous medium. In terms of the porosity ε (defined as the relative volume fraction of discrete phase medium to continuous medium), thermal conductivity k_p and pore shape factor β, the thermal conductivity (k_c) of the continuous medium is altered as:

$$\frac{k_e - k_p}{k_c - k_p}\left(\frac{k_c}{k_e}\right)^{1-2/(3\beta)} = 1 - \varepsilon \quad (15)$$

where k_e is the effective thermal conductivity of the bulk heterogeneous medium. For low conducting gaseous pores distributed randomly within a continuous medium satisfying $k_c >> k_p$, Eq. (15) reduces to:

$$k_e = k_c(1-\varepsilon)^{3\beta/2} \quad (16)$$

For porous media, Gibson and Ashby [18] argued that the specific heat, latent heat and other physical properties remain unaffected by pore inclusions whilst the effective density ρ_e becomes:

$$\rho_e = \rho_c(1-\varepsilon) \quad (17)$$

Correspondingly, the effective thermal diffusivity takes the form:

$$\alpha_e = f\alpha_c = \alpha_c(1-\varepsilon)^{(3\beta/2)-1} \quad (18)$$

Similar to the case of effective thermal conductivity, for low conducting spherical or circular pores, (18) is reduced to $\alpha_e = \alpha_c(1-\varepsilon)^{1/2}$ [15].

The instantaneous temperature distribution in the melt as well as the location of solid–liquid interface within a porous medium may be obtained by substituting the effective thermal conductivity of Eq. (16), the effective density of Eq. (17) and the effective thermal diffusivity of Eq. (18) into the corresponding solutions for a homogeneous medium, yielding:

$$T_s(x,t) = T_m + \frac{2q''_w}{k_e}\sqrt{\alpha_e t\left[ierfc\left(\frac{S(t)}{2\sqrt{\alpha_e t}}\right) - ierfc\left(\frac{x}{2\sqrt{\alpha_e t}}\right)\right]} \quad (19)$$

$$\frac{dS(t)}{dt} = \frac{q''_w}{\rho_e L}erfc\left(\frac{S(t)}{2\sqrt{\alpha_e t}}\right) \quad (20)$$

$$\frac{d\xi}{d\tau_e} = Ste''_e erfc\left(\frac{\xi}{2\sqrt{\tau_e}}\right) \quad (21)$$

where $Ste''_e = c_p H(q''_w/k_e)/L$.

Finally, under the assumptions made above for the present model, the exact solutions for the transient temperature distribution and phase interface location of a semi-infinite heterogeneous

medium containing randomly distributed stagnant pores subject to constant heat flux at the boundary ($x = 0$) are obtained as:

$$T_s(x,t) = T_m + \frac{2q''_w}{(1-\varepsilon)^{3\beta/2}k_s}\sqrt{(1-\varepsilon)^{(3\beta/2)-1}\alpha_s t}\left(ierfc\left(\frac{S(t)}{2\sqrt{(1-\varepsilon)^{(3\beta/2)-1}\alpha_s t}}\right) - ierfc\left(\frac{x}{2\sqrt{(1-\varepsilon)^{(3\beta/2)-1}\alpha_s t}}\right)\right) \quad (22)$$

$$\frac{d\xi}{d\tau_s} = \frac{1}{1-\varepsilon}Ste''erfc\left(\frac{\xi}{2\sqrt{(1-\varepsilon)^{(3\beta/2)-1}\tau_s}}\right) \quad (23)$$

3. Numerical simulation

Due to difficulties associated with the experimentation for solidification in heterogeneous media, it is imperative to perform numerical simulations to validate the analytical model. To this end, the finite difference method (FDM) embedded within a commercially available software Flow-3D™ is employed. The numerically generated model for a continuous medium containing randomly distributed circular pore inclusions is shown in Fig. 2. The two-phase medium is initially at melting temperature, with fixed cooling heat flow at $x = 0$ and adiabatic at $x = H$ as thermal boundary conditions. To ensure 1D heat flow along the x-axis (Fig. 2), the boundaries in other directions are taken as symmetric. For simplicity, two-dimensional (2D) circular pores with varying sizes and adiabatic pore boundaries are considered.

MATLAB™ is used to generate data for pores having different sizes and spatial locations, followed by solid model generation using a commercial computer aided design software – Solidworks™. The solid model is then imported for FDM simulations. It should be noted that, to generate circular pores having desirable random sizes, the upper and lower limits were set as 5.0 mm and 0.64 mm, respectively.

With the convection term and internal heat generation neglected, the governing equation for transient heat conduction with a moving boundary may be expressed as [19]:

$$\frac{\partial \widehat{H}}{\partial t} = \nabla\cdot(k\nabla T) \quad (24)$$

where $\widehat{H}$ denotes the sum of sensible enthalpy $\widehat{h}$ and the latent heat of fusion $\Delta\widehat{H}$, namely the total enthalpy:

$$\widehat{H} = \widehat{h} + \Delta\widehat{H} = \left(\rho\widehat{h}_{ref} + \int_{T_{ref}}^{T}\rho c_p dT\right) + (1-f_L)\rho L \quad (25)$$

Here, c_p is the specific heat at constant pressure, ρ is the density, L defines the latent heat of fusion, and the reference temperature T_{ref} and enthalpy $\widehat{h}_{ref}$ are chosen as those corresponding to the melting temperature according to the manual of FLOW-3D™ [20]. The solid fraction f_s in the enthalpy equations is defined here as:

$$f_s = \begin{cases} 1 & \text{at} \quad T < T_{solidus} \quad \text{solid} \\ \dfrac{T_{liquidus} - T}{T_{liquidus} - T_{solidus}} & \text{at} \quad T_{solidus} < T < T_{liquidus} \quad \text{mushy} \\ 0 & \text{at} \quad T > T_{liquidus} \quad \text{liquid} \end{cases} \quad (26)$$

In the FDM simulations, it is assumed that local thermal equilibrium is in force at the boundary between the pores and the surrounding dense material. Fig. 2 presents a typical snapshot of the simulated solid–liquid interface movement. It is seen that the interface separating the solid and liquid phases is not as straight as that for dense materials. Further, as expected, the interface is perpendicular to the pore boundary as the pores are taken as non-conducting.

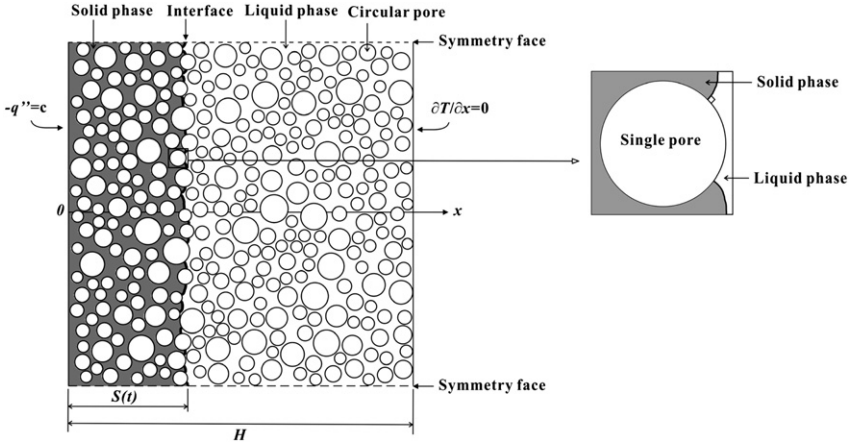

Fig. 2. Finite difference method (FDM) model for solidification process with constant heat flux thermal boundary ($Ste'' = 0.06$) at fixed time $\tau = 3.077$.

4. Discussion of results

4.1. Temporal variation of phase interface

Upon initiating cooling (constant heat flux) at $x = 0$, the melt in the vicinity of the wall begins to solidify. The solidified layer is gradually thickened along the x-axis, indicating that the liquid–solid interface progresses with time away from the boundary. The evolution of this phase interface, represented by its dimensionless location ξ, follows the trend as plotted in Fig. 3. In addition to homogeneous medium ($\varepsilon = 0$), a heterogeneous medium having randomly distributed non-conducting pores that occupy 50% of the total volume (i.e., $\varepsilon = 0.5$) is also considered. With water taken as the continuous medium, both the analytical model predictions and numerical simulation results employing water as presented in Fig. 3. The derivation between analytical prediction and numerical simulation is estimated to be within 4%. With good agreement achieved, the following discussion is solely based upon the prediction results from the present analytical model.

For $\varepsilon = 0$, the solidified layer is thickened non-linearly, i.e., the rate of solidified layer thickening is slightly decreased, even though the trend shown in Fig. 3 appears to be linear. For a given Ste'' number (e.g., $Ste'' = 0.06$), this decrease mainly results from the reduced heat flux at the solid–liquid interface. Fig. 4(a) shows that the heat flux at the interface decreases with time until the liquid phase is fully solidified. It is interesting to notice that even full solidification is reached, the heat flux at $x = H$ is non-zero due to latent heat liberation at the interface.

It is clearly seen from Fig. 3 that the presence of non-conducting (or very low conducting) pores in a homogeneous medium accelerates its solidification, which is distinctively different from the deceleration of solidification under constant temperature thermal boundary (see details [14–16]). At a given time, the solidified layer of the heterogeneous medium ($\varepsilon = 0.5$) is thicker than that of the homogeneous medium ($\varepsilon = 0$). During the process of phase change, the heat flux at the interface is mainly contributed by latent heat liberation: for a given homogeneous medium ($\rho_s = \text{const.}$), a larger heat flux at the interface ($k_s(\partial T_s/\partial x) = \rho_s L(\mathrm{d}S/\mathrm{d}t)$) leads to faster movement of the phase interface. However, the results of Fig. 4(a) show the opposite trend, namely, the heterogeneous medium has a lower heat flux at the interface and its solidification progresses faster relative to that of the homogeneous medium. The heat per unit mass, Q/m (W/kg) or specific heat flow at the phase interface

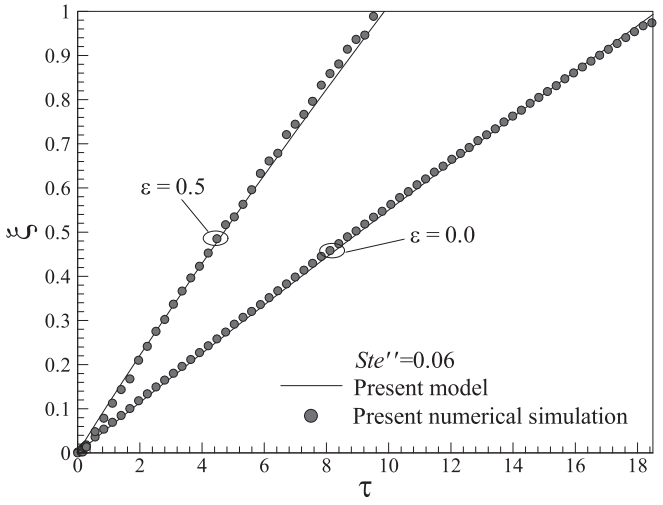

Fig. 3. Analytical and numerical predictions of temporal evolution for solidification front with constant heat flux thermal boundary ($Ste'' = 0.06$).

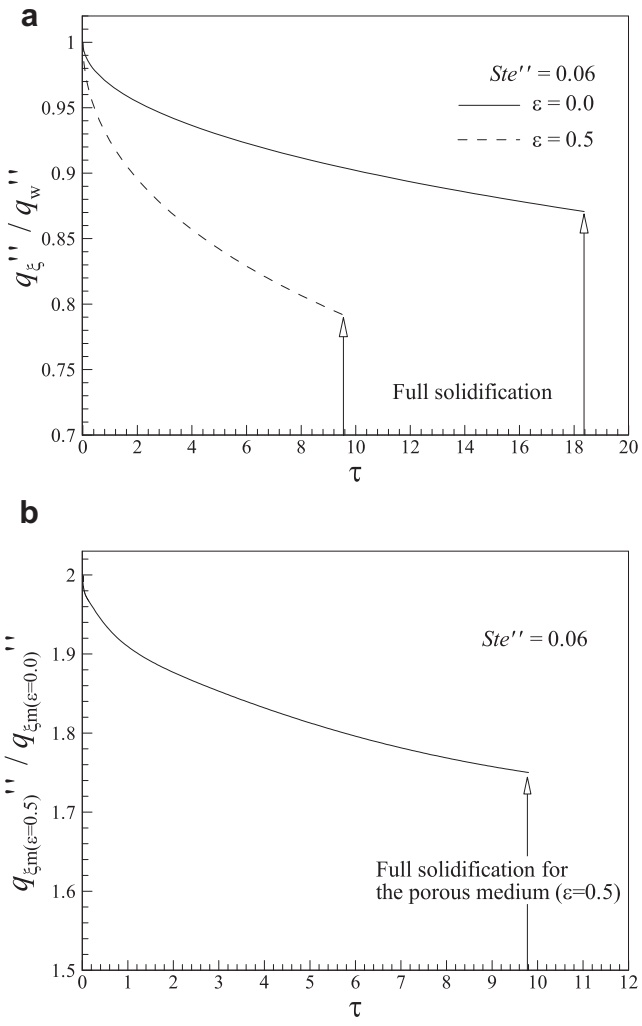

Fig. 4. Variation of (a) heat flow per unit area (W/m^2) and (b) heat flow per unit mass (W/kg) defined as Q/m at phase interface front with time for $Ste'' = 0.06$.

($k_e((\partial T_e/\partial x)/\rho_e) = L(\mathrm{d}S/\mathrm{d}t)$) is thought to be responsible (Fig. 4(b)) since the effective density is reduced with the inclusion of pores. For $\varepsilon = 0.5$, the specific heat flow is approximately twice as high as that of the homogeneous medium.

The accelerated solidification by non-conducting pores may also be explained using energy conservation argument. For a solidified layer including the phase interface and the boundary, energy conservation dictates that:

$$Q_{boundary} = Q_{latent} + Q_{sensible} = \rho_e\left(L\Delta S + c_p V \Delta T\right) \tag{27}$$

where S represents the thickness of the solidified layer, V is the relative volume, and ρ_e and L are the effective density and latent heat of the heterogeneous medium, respectively. With pore inclusion ($\varepsilon = 0.5$), whilst the effective density is reduced as indicated by Eq. (17), both $L\Delta S$ (latent heat) and $Vc_p\Delta T$ (sensible heat) increase as expressed in Eq. (27). The maximum ratio of sensible heat to latent heat is calculated to be 0.15 and 0.265 for the homogeneous medium and heterogeneous medium ($\varepsilon = 0.5$), respectively, demonstrating the dominant role of latent heat in the phase change process. Therefore, the heat liberated at the phase interface during phase change should be increased further to satisfy the constant heat flux at the boundary. This, in turn, increases ΔS with invariant

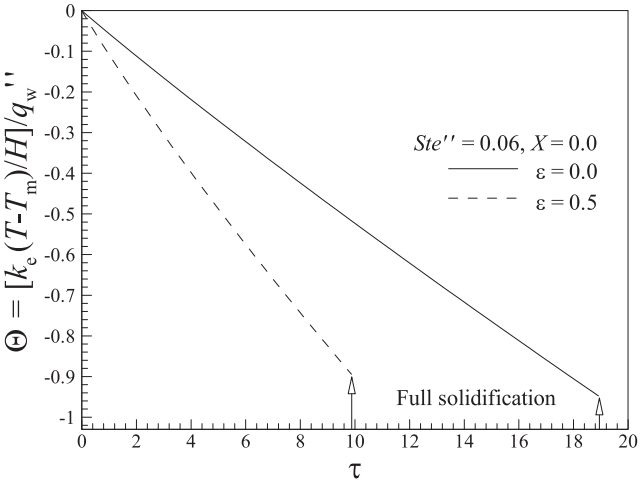

Fig. 5. Variation of surface temperature at the boundary ($X = 0$) for both homogeneous medium and heterogeneous medium ($\varepsilon = 0.5$) at $Ste'' = 0.06$.

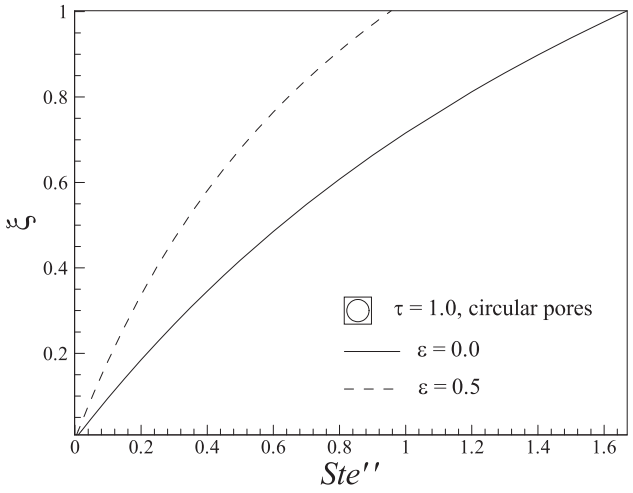

Fig. 7. Influence of Stefan number upon temporal phase interface location for both homogeneous medium and heterogeneous medium ($\varepsilon = 0.5$, circular pores) at $\tau = 1.0$.

V and L and hence explains the accelerated solidification in the presence of pore inclusions.

4.2. Temperature distribution in solidified layer and cooling rate at boundary

The present analytical model provides an estimate of local temperature distribution in the solidified layer as well as cooling rate at the boundary of a heterogeneous medium. The local temperature normalized by the prescribed constant heat flux is expressed as:

$$\Theta = [k_e(T - T_m)/H]/q''_w = 2\sqrt{\tau_e\left[ierfc\left(\frac{\xi}{2\sqrt{\tau_e}}\right) - ierfc\left(\frac{X}{2\sqrt{\tau_e}}\right)\right]} \quad 0 \le X \le \xi \tag{28}$$

where $X = x/H$, and $\tau_e = \tau_s(1 - \varepsilon)^{(3\beta/2)-1}$ is the dimensionless solidification time for the heterogeneous medium.

The predicted variation of surface temperature at the boundary ($X = 0$) is plotted as a function of time for both the homogeneous and heterogeneous media with fixed cooling condition, $Ste'' = 0.06$ (see Fig. 5). The temperature is seen to decrease linearly with time and, at any given time, the rate of decrease is greater for the heterogeneous medium. This implies that the cooling rate ($|\Delta\Theta/\Delta\tau|$) at the boundary is higher if non-conducting pores are included. Mukherjee et al. [21] demonstrated that the variation in cooling rate – defined as temperature drop per second (K/s) – during the fabrication of closed-cell aluminum foams strongly influences the compressive strength of the foam by changing micro- and macro-cell topologies. Their experimental results showed that a higher cooling rate reduces the cell size and increases the compressive strength of the foam. Therefore, for the processing of closed-cell metallic foams via the foaming route, the presence of pores will always increase foam compressive strength if constant heat flow is imposed at the boundary for the purpose of cooling.

4.3. Effect of pore shape on phase interface location

The present analysis has thus far been performed based on the assumption of randomly distributed circular pores. For closed-cell aluminum foams, the shape of pore varies with porosity [22]. For constant wall temperature boundary condition, it has been established that pore shape alters the solidification behavior, as it

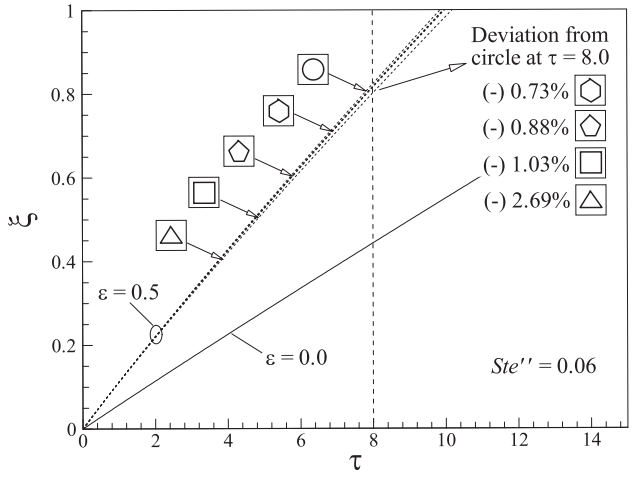

Fig. 6. Influence of pore shape upon temporal phase interface location for $Ste'' = 0.06$.

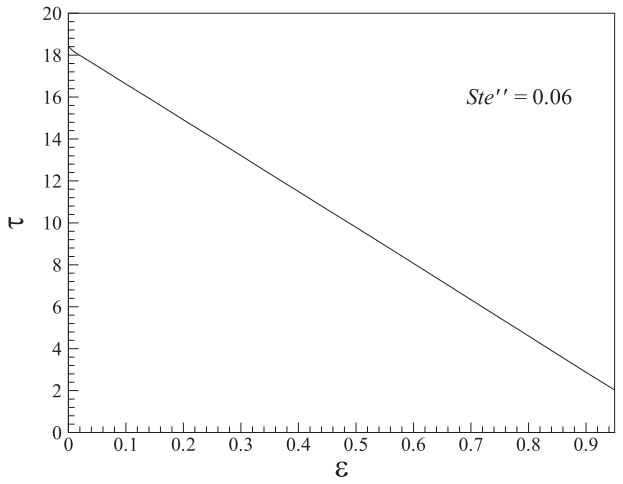

Fig. 8. Influence of porosity on full solidification time for $Ste'' = 0.06$.

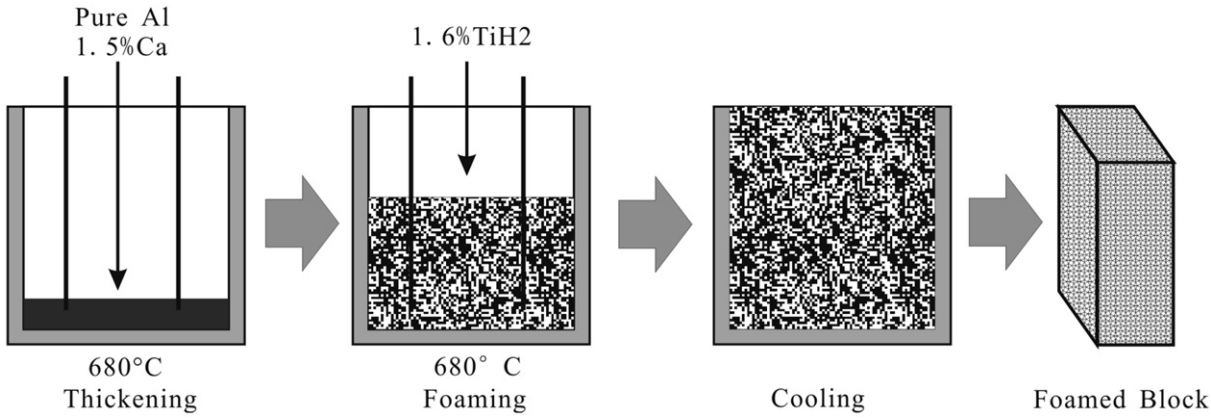

Fig. 9. Direct foaming technique for closed-cell metallic foams [25].

influences significantly of the effective thermal conductivity even if the porosity is fixed [15]. Whether this holds for constant heat flux boundary condition is clarified below.

The results presented in Fig. 6 suggest that, for the types of pore considered in this study (triangle, square, pentagon, hexagon and circle), pore shape does not play a significant role in solidification: the evolution of phase interface is almost insensitive to pore shape. For the five selected pore shapes, the phase interfaces seem to behave in a very similar manner, collapsing onto a single curve. For example, with the porosity fixed at 0.5, whilst the thermal conductivity is decreased by about 30.5% when the pore shape is changed from a circle to a triangle, the thickening of the solidified layer is decreased by only 2.69% at $\tau = 8.0$ (for more details, see Fig. 6).

The above observation indicates the marginal role of effective thermal conductivity in determining the temporal evolution of phase change interface, supporting the argument reported in references [23,24] that, for a given porosity, the change in pore shape acts to vary the effective thermal conductivity but not the effective density. This further implies that the effective density determines the evolution of phase interface during phase change.

4.4. Effect of Stefan number on phase interface location

The level of heat flux removed from the boundary (i.e., $x = 0$) is expressed as $Ste'' = (c_p H q''/k_s)/L$. The influence of Ste'' on phase change interface for both homogeneous and heterogeneous media is considered in this section. Fig. 7 depicts how the phase interface evolves with varying cooling heat flux at the boundary.

For a given medium (either dense or porous), the phase change interface propagates faster as the cooling heat flux is increased, following the trend in Fig. 7, and the growth rate of the solidified layer is considerably reduced as the Ste'' number is increased. The heterogeneous medium ($\varepsilon = 0.5$) reaches full solidification earlier than the dense material. The solidified layer of the porous medium ($\varepsilon = 0.5$) having circular pores is approximately 3 times (for $Ste'' = 0.2$) and 5 times (for $Ste'' = 0.4$) thicker than that with $Ste'' = 0.06$ at $\tau = 1.0$.

4.5. Effect of porosity on full solidification time

The present analysis has considered hitherto phase change behavior for a fixed porosity ($\varepsilon = 0.5$). It is apparent that the variation in porosity can significantly influence the bulk properties of a heterogeneous medium, altering the phase change characteristics such as the evolution of phase interface, full solidification time, and temperature distribution in the solidified layer.

As the porosity is increased, the full solidification time is remarkably reduced as plotted in Fig. 8. The full solidification of the heterogeneous medium is, for example, twice (for $\varepsilon = 0.71$) and 3 times (for $\varepsilon = 0.8$) shorter than that required for the homogeneous medium. As previously discussed, subject to the present constant heat flux boundary condition, the effective density of the bulk medium governs the evolution of phase change interface. The increased porosity reduces the effective density of the bulk medium, resulting in the decreased time required for full solidification, indicating that the inclusion of non-conducting pores accelerates significantly the phase change. It is worth noting that a mathematical singularity exists when the porosity is unity ($\varepsilon = 1.0$), as no phase change material exists.

4.6. Practical importance

A typical fabrication route of closed-cell aluminum foams is the direct foaming [25] as illustrated in Fig. 9 where calcium is firstly added to aluminum melt at 680 °C then stirred for several minutes whilst its viscosity continuously increases up to a desirable value due to the formation of calcium oxide (CaO). Consequently, the melt becomes highly viscous enough to prevent the gaseous bubbles from floating to the top. Subsequently, TiH_2 which serves as the blowing agent by releasing hydrogen is added to the melt. The melt soon starts to expand slowly and gradually fills the foaming vessel. As the vessel is cooled below the melting temperature of the mixture, the melt foam turns into solid state.

It has been demonstrated [26,27] that closed-cell aluminum foams with different pore morphologies exhibit different load-bearing and energy-absorbing properties. Porosity, pore size and pore shape are the three main factors controlling the cellular morphology of a closed-cell metallic foam, which is influenced by many processing factors such as foaming time (i.e., cooling effectiveness) [22,28]. To better understand such complicated foaming and solidification process, the solidification behavior of heterogeneous media having randomly-distributed circular pores with negligible thermal conductivity under various thermal boundary conditions needs to be fully explored.

One of the idealized yet significant thermal boundary conditions, constant heat flux provides the lower bound for the solidification process. It should be noted that under all the other thermal boundary conditions e.g., constant wall temperature boundary condition, the wall heat flux decreases with time. The present finding suggests that for fabricating closed-cell aluminum foams, the constant heat flux-like boundary condition can provide relatively short full solidification time compared to any other thermal

boundary conditions for given morphologies. Such faster cooling of the melt with pores, which could be achieved by imposing the constant heat flux thermal boundary, is also known to increase the foam compressive strength of the final closed-cell metallic foams via the direct foaming route (Mukherjee et al. [20]).

5. Conclusions

An analytical model capable of predicting the temporal phase interface front of heterogeneous media with constant heat flux boundary has been introduced. The model was developed by combining an existing one-dimensional solidification model for homogeneous media and an effective thermal conductivity model for porous media. For validation, numerical simulations on both homogeneous medium and heterogeneous medium (dense medium containing randomly distributed non-conducting gaseous pores) were conducted. Good agreement (derivation within 4%) between model predictions and numerical simulations is achieved.

Conclusions drawn from present study are summarized as follows:

(1) The solidification front evolves faster with the inclusion of non-conducting pores, thickening the solidified layer as a result of decreased effective density of the bulk medium.
(2) The cooling rate of the heterogeneous medium is much higher than that of the homogeneous medium.
(3) The evolution of phase change interface is insensitive to variation in pore shape, indicating that the effective thermal conductivity plays a minor role in the phase change process.
(4) Increasing the Ste'' number (by increasing the cooling heat flow) increases considerably the speed of solidification, leading to significant thickening of the solidified layer.
(5) The presence of non-conducting pores in the heterogeneous medium reduces the time required for full solidification, and the time required to fully solidify the heterogeneous medium decreases with increasing porosity.

Acknowledgement

This study is supported by the National Basic Research Program of China (2011CB610305), the National “111” Project of China (B06024), and the National Natural Science Foundation of China (10825210, 11072188 and 51206128).

References

[1] B. Zalba, J.M. Marin, L.F. Cabeza, H. Mehling, Review on thermal energy storage with phase change: materials, heat transfer analysis and applications, Appl. Therm. Eng. 23 (2003) 251–283.
[2] V. Butala, U. Stritih, Experimental investigation of PCM cold storage, Energ. Buildings 41 (2009) 354–359.
[3] M. Akgün, O. AydIn, K. Kaygusuz, Thermal energy storage performance of paraffin in a novel tube-in-shell system, Appl. Therm. Eng. 28 (2008) 405–413.
[4] M.C. Flemings, Solidification processing, Metall. Mater. Trans. B 5 (1974) 2121–2134.
[5] H.S. Carslaw, J.C. Jaeger, Conduction of Heat in Solids, second ed. Clarendon Press, Oxford, 1959.
[6] M.S. El-Genk, A.W. Cronenberg, Solidification in a semi-infinite region with boundary conditions of the second kind: an exact solution, Lett. Heat Mass Transf. 6 (1979) 321–327.
[7] T.R. Goodman, The heat-balance integral and its application to problems involving a change of phase, Trans. ASME 80 (1958) 335–342.
[8] K. Stephan, B. Holzknecht, Perturbation solutions for solidification problems, Int. J. Heat Mass Transf. 19 (1976) 597–602.
[9] A. London, R. Seban, Rate of ice formation, Trans. ASME 65 (1943) 771–779.
[10] F. Megerlin, Geometrisch eindimensionale wärmeleitung beim schmelzen und erstarren, Forsch. Ingenieur. 34 (1968) 40–46.
[11] R. Siegel, J.M. Savino, An analysis of the transient solidification of a flowing warm liquid on a convectively cooled wall, in: Proceedings of The Third Chemical Engineers, New York, 1966.
[12] S. Lin, Z. Jiang, An improved quasi-steady analysis for solving freezing problems in a plate, a cylinder and a sphere, J. Heat Transf. 125 (2003) 1123.
[13] E. Eckert, R. Goldstein, W. Ibele, S. Patankar, T. Simon, P. Strykowski, K. Tamma, T. Kuehn, A. Bar-Cohen, J. Heberlein, Heat transfer: a review of 1994 literature, Int. J. Heat Mass Transf. 40 (1997) 3729–3804.
[14] B. Zhang, T. Kim, T.J. Lu, The solidification of two-phase heterogeneous materials: theory versus experiment, Sci. China, Ser. E (Technol. Sci.) 52 (2009) 1688–1697.
[15] B. Zhang, T. Kim, T.J. Lu, Analytical solution for solidification of close-celled metal foams, Int. J. Heat Mass Transf. 52 (2009) 133–141.
[16] B. Zhang, T. Kim, T.J. Lu, Solidification in a continuous medium with periodically distributed two-dimensional circular pores, J. Thermophys. Heat Transf. 24 (2010) 348–354.
[17] T. Bauer, A general analytical approach toward the thermal conductivity of porous media, Int. J. Heat Mass Transf. 36 (1993) 4181–4191.
[18] L.J. Gibson, M.F. Ashby, Cellular Solids: Structure and Properties, second ed. Cambridge University Press, 1999.
[19] V. Voller, Fast implicit finite-difference method for the analysis of phase change problems, Numer. Heat Transf., Part B 17 (1990) 155–169.
[20] C. Hirt, B. Nichols, Flow-3D User's Manual, Flow Science Inc., 2005.
[21] M. Mukherjee, U. Ramamurty, F. Garcia-Moreno, J. Banhart, The effect of cooling rate on the structure and properties of closed-cell aluminium foams, Acta Mater. 58 (2010) 5031–5042.
[22] Q.C. Zhang, T.J. Lu, S.Y. He, D.P. He, Control of pore morphology in close-celled aluminium foams, J. Xi'an Jiaotong Univ. 41 (2007) 255–270.
[23] J. Wang, J.K. Carson, M.F. North, D.J. Cleland, A new approach to modeling the effective thermal conductivity of heterogeneous materials, Int. J. Heat Mass Transf. 49 (2006) 3075–3083.
[24] M. Kaviany, Principles of Heat Transfer in Porous Media, second ed. Springer-Verlag, New York, 1995.
[25] J. Banhart, Manufacture, characterisation and application of cellular metals and metal foams, Prog. Mater. Sci. 46 (2001) 559–632.
[26] Y. Zhou, D.P. He, J.Q. Jiang, New type of spherical pore Al alloy foam with low porosity and high strength, Sci. Chin. Ser. B 47 (2004) 407–413.
[27] D.H. Yang, D.P. He, Thermal decomposition properties of titanium hydride and Al alloy foam with low porosity and small pore diameter, Chin. J. Nonferr. Meth. 14 (2004) 2021–2028.
[28] H. Stanzick, M. Wichmann, J. Weise, L. Helfen, T. Baumbach, J. Banhart, Process control in aluminum foam production using real-time X-ray radioscopy, Adv. Eng. Mater. 4 (10) (2002) 814–823.